Collective nuclear excitations with Skyrme-second random-phase approximation

D. Gambacurta,[1,2,*] M. Grasso,[3] and F. Catara[1,2]
[1]*Dipartimento di Fisica e Astronomia dell'Universitá di Catania, Via S. Sofia 64, I-95123 Catania, Italy*
[2]*Istituto Nazionale di Fisica Nucleare, Sezione di Catania, Via S. Sofia 64, I-95123 Catania, Italy*
[3]*Institut de Physique Nucléaire, Université Paris-Sud, IN2P3-CNRS, F-91406 Orsay Cedex, France*
(Received 22 February 2010; published 20 May 2010)

Second random-phase approximation (RPA) calculations with a Skyrme force are performed to describe both high- and low-lying excited states in ^{16}O. The coupling between one particle-one hole and two particle-two hole as well as that between two particle-two hole configurations among themselves are fully taken into account, and the residual interaction is never neglected; we do not resort therefore to a generally used approximate scheme where only the first kind of coupling is considered. The issue of the rearrangement terms in the matrix elements beyond the standard RPA will be considered in detail in a forthcoming paper. Two approximations are employed here for these rearrangement terms: they are either neglected or evaluated with the RPA procedure. As a general feature of second RPA results, a several-MeV shift of the strength distribution to lower energies is systematically found with respect to RPA distributions. A much more important fragmentation of the strength is also naturally provided by the second RPA owing to the huge number of two particle–two hole configurations. A better description of the excitation energies of the low-lying 0^+ and 2^+ states is obtained with the second RPA than with the RPA.

DOI: 10.1103/PhysRevC.81.054312 PACS number(s): 21.10.Re, 21.60.Jz

I. INTRODUCTION

The random-phase approximation (RPA) is currently used to describe the excitation spectrum of a quantum many-body system. Its success in nuclear physics is well established, and the method has been applied for many years to describe giant resonances and low-lying excitation modes. However, this approach presents some well-known limitations. Extensions and procedures to go beyond the RPA and to improve the treatment of the correlations present in a many-body system have been introduced in the past decades. A first natural extension is the quasiparticle RPA (QRPA), where pairing correlations are included by defining quasiparticle states through the unitary Bogoliubov transformations [1]. This allows a description of the excitation modes in superfluid open-shell nuclei.

Other types of correlation may be introduced in a different framework. A weak point in the formal development of the RPA is related to the use of the quasiboson approximation (QBA) which implies a violation of the Pauli principle as well as a severe approximation on the reference state: the uncorrelated Hartree-Fock (HF) ground state is used in place of the correlated one. An explicitly correlated ground state as reference state is employed in those extensions of the RPA where either the use of the QBA is avoided or its effects are cured. Several examples of these beyond-RPA methods have been discussed in recent decades (see, e.g., [2] and references therein).

Another natural extension of the RPA, also based on the QBA, is the second RPA (SRPA) method where two particle–two hole ($2p2h$) excitations are included together with the usual RPA one particle–one hole ($1p1h$) configurations, providing in this way a richer description of the excitation modes. The SRPA equations have been well known for many years and have been derived by following different procedures. Some examples are the derivation within the equations-of-motion method [3] and the procedures employing a variational approach [4] or the small-amplitude limit of the time-dependent density matrix [5,6]. However, until very recently, the SRPA equations have never been fully and self-consistently solved because of the heavy numerical effort they require. Some approximations have been adopted in the past; namely, the SRPA equations have been reduced to a simpler second Tamm-Dancoff model (i.e., the matrix B is put equal to zero; see, for instance, [7–10]) and/or the equations have been solved with uncorrelated $2p2h$ states: the residual interaction terms in the matrix that couples $2p2h$ configurations among themselves have been neglected (diagonal approximation) [11–17]. Very recently, this problem has regained a new interest; it is becoming numerically more accessible now, and the SRPA equations have been solved for closed-shell nuclei using an interaction derived from the Argonne V18 potential (with the unitary correlation operator method) [18,19] and for small metallic clusters in the jellium approximation [20].

The increasing interest in the context of nuclear structure is also justified by the manifestation of new phenomena in unstable nuclei. For instance, pygmy resonances represent exotic low-lying excitation modes related to the presence of a skin in neutron-rich nuclei. The necessity to go beyond the standard mean field to describe these resonances has been demonstrated by the important effects found when particle-vibration coupling is included [22].

In the SRPA, the coupling of the $1p1h$ configurations with the $2p2h$ ones is fully considered, providing thus a more general description of excited states than the one obtained in the standard RPA. Some excitations like the giant or pygmy resonances may already be described at the RPA level by using the standard $1p1h$ configurations. The introduction of $2p2h$ configurations is expected in these cases to enrich

*Danilo.Gambacurta@ct.infn.it

the theoretical description, providing an eventual shift of the excitation energy and a proper treatment of the widths. Other states, like the first 0^+ or 2^+ states in magic nuclei, are not reproduced by the standard RPA model because configurations beyond $1p1h$ are needed to describe them. Finally, $2p2h$ configurations would allow one to study in a proper way the double-phonon excitation modes that are experimentally well known in nuclei [23] and have been the object of several theoretical analyses. Most of these studies have so far been based on boson mapping procedures, which, however, require high-order expansions in order to take into account the corrections owing to the Pauli principle (see Ref. [24] and references therein). In many of the above-mentioned collective excitations, the $2p2h$ components might have a very important role, and thus interesting results are expected from the application of the SRPA, including all kinds of coupling between $1p1h$ and $2p2h$ elementary excitations.

The most often employed phenomenological interactions currently in nuclear mean-field models are density-dependent forces of Skyrme or Gogny type. It is well known that, with density-dependent forces, the residual interaction used to evaluate the RPA matrices A and B contains a rearrangement term coming from the derivative with respect to the density of the mean-field Hamiltonian (the second derivative of the energy density functional). A first formal aspect to consider in the SRPA problem with density-dependent forces is the determination of the residual interaction that has to be used in the matrix elements that are new with respect to the RPA. To our knowledge, this aspect has not yet been clarified in the literature. A prescription is introduced in Ref. [25], and rearrangement terms appear in the matrix elements beyond the RPA. However, in more recent calculations [26], the same authors did not actually use that prescription and did not include those rearrangement terms. For the results shown here, we have explored two possibilities: (i) We have not included rearrangement terms in beyond-RPA matrix elements; (ii) we have calculated them with the usual RPA prescription. In a forthcoming paper, we will discuss in more detail the formal derivation of the residual interaction in the context of the SRPA with density-dependent interactions.

To our knowledge, current versions of the SRPA are based on noninteracting $2p2h$ configurations, and only the interaction between $2p2h$ and $1p1h$ comfigurations has generally been taken into account, in the so-called diagonal approximation. In this work, we present full (the diagonal approximation is not employed and the matrix B is different from zero) Skyrme-SRPA results obtained for the doubly magic nucleus ^{16}O. In Sec. II the formal scheme of the SRPA is briefly summarized, and the use of the QBA in the context of the SRPA is commented on. Numerical checks on stability and sum rules are presented in Sec. III. Results are shown in Sec. IV, and a comparison between RPA and SRPA excitation spectra is made for both giant resonances and low-lying states in ^{16}O. In particular, for the giant resonances, the transition densities are analyzed and the radial distributions related to the main peaks are shown for the RPA and SRPA. For the low-lying states, special interest is devoted to the first 0^+ and 2^+ excitation modes. They are mainly composed of $2p2h$ configurations and, for this reason, cannot be correctly predicted by the RPA. A comparison of the full SRPA results with those obtained in the diagonal approximation is also presented. Conclusions and perspectives are finally discussed in Sec. V.

II. FORMAL SCHEME

We briefly recall the main formal aspects of the SRPA that can be found in several articles (see, for instance, Ref. [3]). The SRPA is a natural extension of the RPA where the excitation operators Q^+_ν are a superposition of $1p1h$ and $2p2h$ configurations:

$$Q^\dagger_\nu = \sum_{ph} \left(X^\nu_{ph} a^\dagger_p a_h - Y^\nu_{ph} a^\dagger_h a_p\right) + \sum_{p<p',h<h'} \left(X^\nu_{php'h'} a^\dagger_p a_h a^\dagger_{p'} a_{h'} - Y^\nu_{php'h'} a^\dagger_h a_p a^\dagger_{h'} a_{p'}\right). \tag{1}$$

The X's and Y's are solutions of the equations

$$\begin{pmatrix} \mathcal{A} & \mathcal{B} \\ -\mathcal{B}^* & -\mathcal{A}^* \end{pmatrix} \begin{pmatrix} \mathcal{X}^\nu \\ \mathcal{Y}^\nu \end{pmatrix} = \omega_\nu \begin{pmatrix} \mathcal{X}^\nu \\ \mathcal{Y}^\nu \end{pmatrix}, \tag{2}$$

where

$$\mathcal{A} = \begin{pmatrix} A_{11} & A_{12} \\ A_{21} & A_{22} \end{pmatrix}, \quad \mathcal{B} = \begin{pmatrix} B_{11} & B_{12} \\ B_{21} & B_{22} \end{pmatrix},$$
$$\mathcal{X}^\nu = \begin{pmatrix} X^\nu_1 \\ X^\nu_2 \end{pmatrix}, \quad \mathcal{Y}^\nu = \begin{pmatrix} Y^\nu_1 \\ Y^\nu_2 \end{pmatrix}.$$

The indices 1 and 2 are a shorthand notation for the $1p1h$ and $2p2h$ configurations, respectively. The usual RPA matrices are denoted A_{11} and B_{11}, A_{12} and B_{12} are the matrices coupling $1p1h$ with $2p2h$ configurations, and A_{22} and B_{22} are the matrices coupling $2p2h$ configurations among themselves. If the QBA is used and the HF ground state is thus employed to evaluate these matrix elements, it can be shown that B_{12}, B_{21}, and B_{22} are zero. The other matrix elements are equal to

$$\begin{aligned} A_{12} &= A_{ph,p_1p_2h_1h_2} \\ &= \langle \mathrm{HF}|\left[a^\dagger_h a_p, \left[H, a^\dagger_{p_1} a^\dagger_{p_2} a_{h_2} a_{h_1}\right]\right]|\mathrm{HF}\rangle \\ &= \chi(h_1,h_2)\bar{V}_{h_1pp_1p_2}\delta_{hh_2} - \chi(p_1,p_2)\bar{V}_{h_1h_1p_1h}\delta_{pp_2}, \end{aligned} \tag{3}$$

$$\begin{aligned} A_{22} &= A_{p_1h_1p_2h_2,p'_1h'_1p'_2h'_2} \\ &= \langle \mathrm{HF}|\left[a^\dagger_{h_1} a^\dagger_{h_2} a_{p_1} a_{p_2}, \left[H, a^\dagger_{p'_2} a^\dagger_{p'_1} a_{h'_2} a_{h'_1}\right]\right]|\mathrm{HF}\rangle \\ &= \left(\epsilon_{p_1} + \epsilon_{p_2} - \epsilon_{h_1} - \epsilon_{h_2}\right)\chi(p_1,p_2)\chi(h_1,h_2) \\ &\quad \times \delta_{h_1h'_1}\delta_{p_1p'_1}\delta_{h_2h'_2}\delta_{p_2p'_2} + \chi(h_1,h_2)\bar{V}_{p_1p_2p'_1p'_2}\delta_{h_1h'_1}\delta_{h_2h'_2} \\ &\quad + \chi(p_1,p_2)\bar{V}_{h_1h_2h'_1h'_2}\delta_{p_1p'_1}\delta_{p_2p'_2} \\ &\quad + \chi(p_1,p_2)\chi(h_1,h_2)\chi(p'_1,p'_2)\chi(h'_1,h'_2) \\ &\quad \times \bar{V}_{p_1h'_1h_1p'_1}\delta_{h_2h'_2}\delta_{p_2p'_2}, \end{aligned} \tag{4}$$

where the ϵ's are the HF single-particle energies, $\bar{V}$ is the residual interaction, and $\chi(ij)$ is the antisymmetrizer for the indices i,j.

It can be shown [4,14], that the SRPA problem can be reduced to an energy-dependent, RPA-like, eigenvalue problem but where the A_{11} RPA matrix depends on the excitation energies,

$$A_{1,1'}(\omega) = A_{1,1'} + \sum_{2,2'} A_{1,2}(\omega + i\eta - A_{2,2'})^{-1} A_{2',1'}. \quad (5)$$

To calculate this energy-dependent part, one has to invert the A_{22} matrix defined in Eq. (4), whose dimensions are generally very large, requiring thus a strong numerical effort. However, if the terms depending on the residual interaction are neglected, resorting to the so-called diagonal approximation, the inversion is algebraic. This approximation, often used in SRPA calculations, will be analyzed in Sec. IV.

Expressions (3) and (4) are valid in cases where the interaction is not density dependent. Rearrangement terms should be included in the case of density-dependent forces. To obtain the results discussed in Sec IV, (i) we have calculated the matrix elements (3) and (4) with $V = V(\rho_0)$ (ρ_0 being the HF density) without any rearrangement terms, and (ii) we have evaluated them by adding the usual RPA rearrangement contributions also in the A_{12} and A_{22} matrices.

It can be shown that the energy-weighted sum rules (EWSRs) are satisfied in the SRPA [3]. Moreover, the first moment

$$m_1 = \sum_{\nu} \omega_\nu |\langle \nu | F | 0 \rangle|^2 \quad (6)$$

for a generic one-body operator is found to be the same in the RPA and SRPA [27]. A numerical check of this feature is provided in the next section.

Some comments about the use of the QBA in the SRPA can be found in the literature [20,28,29]: it is said that the use of the QBA in the SRPA is a more drastic and severe approximation than in the RPA. This can be easily understood within the variational derivation of the SRPA provided by Providencia [4]. The usual way of writing the RPA ground state is

$$|\Psi\rangle = e^{\hat{S}} |\Phi\rangle, \quad (7)$$

where

$$\hat{S} = \sum_{ph} C_{ph}(t) a_p^\dagger a_h, \quad (8)$$

the operator $\hat{S}$ being a superposition of $1p1h$ configurations built on top of the HF ground state $|\Phi\rangle$. The expression of the SRPA ground state in Ref. [4] is the same as that in Eq. (7), where now the operator $\hat{S}$ also contains $2p2h$ terms:

$$\hat{S} = \sum_{ph} C_{ph}(t) a_p^\dagger a_h + \frac{1}{2} \sum_{php'h'} \hat{C}_{pp'hh'}(t) a_p^\dagger a_{p'}^\dagger a_h a_{h'}. \quad (9)$$

This means that the ground state is no longer a Slater determinant. Because of this, the use of the HF ground state to calculate the matrix elements (QBA) is a stronger approximation than in the RPA. Extensions to cure this problem in the context of the SRPA have been proposed and applied to a simple model [29] and to metal clusters [20]. Future applications to nuclei are in progress.

III. STABILITY OF THE RESULTS AND SUM RULES

In this section we briefly discuss some technical details of the calculations, paying particular attention to the convergence of the results. As a first step, we solved the HF equation in the coordinate space, by using a 20-fm box. In RPA and SRPA calculations we consider the first $n = 7$ single-particle (s.p.) states for each l, with l up to 6. The s.p. wave functions have been represented as linear superpositions of square-well ones. The SGII [21] parametrization of the effective interaction has been used in the present calculations. Since Coulomb and spin-orbit interactions are not taken into account in the residual interaction, our calculations are not fully self-consistent and thus violations of the EWSRs are found (at worst of 5%). The s.p. space has been chosen large enough to assure that the EWSRs are stable. In the following, we will focus our attention on the excitation spectrum up to 50 MeV.

In RPA calculations, $1p1h$ configurations with unperturbed energy up to 100 MeV are considered, while in the SRPA we have considered all the $2p2h$ configurations with an unperturbed energy lower than an energy cutoff $E_{\rm cut}$.

In the SRPA, matrix elements of the residual interaction with three particle–one hole or four-particle indices appear in A_{12} and A_{22}, respectively. Because of the zero-range nature of the interaction, matrix elements involving high-energy single-particle states can also have non-negligible values. We have, however, checked that they do not change too drastically in the energy regions we are interested in. In order to study the stability of the results with respect to the cutoff, we have analyzed how the strength distributions change on increasing $E_{\rm cut}$ from 80 up to 120 MeV.

It is well known that each excitation mode is characterized by an escape ($\Gamma^\uparrow$) and a spreading ($\Gamma^\downarrow$) width as well as by a Landau damping (see, for instance, Ref. [30]). The latter can already be described by a standard discrete RPA calculation. The spreading width cannot be described by the standard RPA, while the SRPA model can take it into account by treating the doorway states as $2p2h$ configurations (providing in this way at least a partial description of the physical widths); the huge number of $2p2h$ configurations makes the SRPA discrete strength distributions much denser than the RPA ones (see Fig. 5). The ($\Gamma^\uparrow$) width is obviously not included in any calculation in a discrete basis. The continuous strength distributions shown in this work are obtained by folding the discrete spectra coming out of our calculations with a Lorentzian having a width of 1 MeV, which is just a smoothing parameter introduced to make easier the comparison between different results. It is not strictly related to the physical width, whose calculation is beyond the scope of the present work.

In Figs. 1 and 2 we show the monopole and quadrupole strength distributions, respectively, for different choices of $E_{\rm cut}$ (indicated in MeV in parentheses in the figures). The multipole transition operators used are

$$F_\lambda^{\rm IS} = \sum r_i^n Y_{\lambda 0}(\hat{r}_i), \quad (10)$$

$$F_\lambda^{\rm IV} = \sum r_i^n Y_{\lambda 0}(\hat{r}_i) \tau_z(i) \quad (11)$$

in the isoscalar and isovector channels, respectively, where $n = \lambda$ except for $\lambda = 0$ where $n = 2$. From the figures, we see

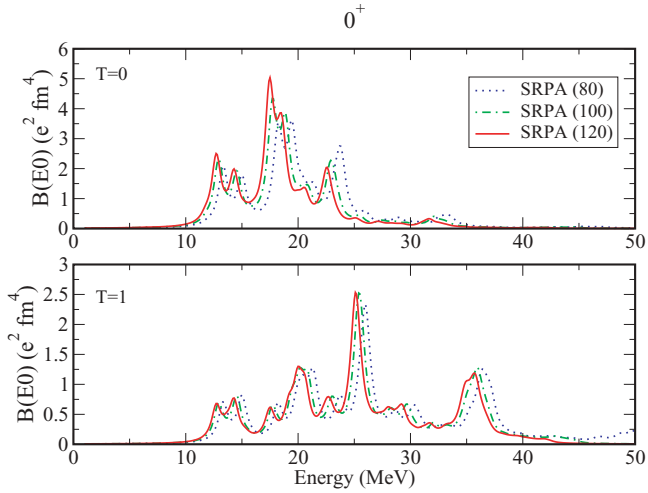

FIG. 1. (Color online) Isoscalar (upper panel) and isovector (lower panel) strength distributions for monopole states obtained in the SRPA for increasing values of the energy cutoff, indicated in MeV in parentheses in the figure, on the $2p2h$ configurations.

that a cutoff equal to 120 MeV is suitable to have stable results. Similar stability checks have been systematically made for all the results shown in the following.

As mentioned above, the EWSRs are satisfied in the SRPA and the first moment (6) is the same in the RPA and SRPA. For a generic one-body operator,

$$F = \sum_{\alpha,\beta} \langle \alpha | F | \beta \rangle a^\dagger_\alpha a_\beta, \tag{12}$$

the transition amplitudes are easily calculated, and they have the same expression in both the RPA and SRPA, namely,

$$\langle 0 | [Q_\nu, F] | 0 \rangle \approx \langle \mathrm{HF} | [Q_\nu, F] | \mathrm{HF} \rangle = \sum_{ph} \left\{ X^{\nu *}_{ph} \langle p | F | h \rangle + Y^{\nu *}_{ph} \langle h | F | p \rangle \right\}. \tag{13}$$

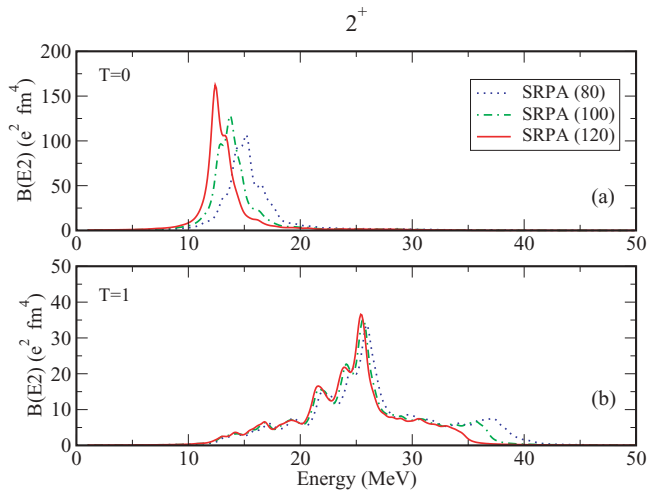

FIG. 2. (Color online) As Fig. 1 but for the quadrupole case.

TABLE I. Evolution of the monopole isoscalar and isovector first moments obtained in the SRPA, (second and third columns, respectively) as a function of the $\omega_{\max}$ parameter in MeV [see Eq. (14)]. In the last row, the corresponding RPA values are reported with $\omega_{\max} = 100$ MeV.

$\omega_{\max}$	$m_1(T=0)$ SRPA	$m_1(T=1)$ SRPA
40	626.4381	115.4153
50	648.9699	147.8026
60	661.0194	182.7364
70	664.3803	193.7896
80	669.7185	197.6874
90	671.4575	200.6472
100	671.6515	201.2473
110	671.6515	201.2473
RPA	671.6516	201.2494

We note that only the p-h components of the transition operator are selected and that, in the case of the SRPA also, only the $1p1h$ amplitudes appear in the above equation.

In the present work, when an energy cutoff $E_{\mathrm{cut}} = 120$ MeV is used on the $2p2h$ configuration, SRPA calculations involve the diagonalization of large matrices, of the order of $N = (5\text{–}6) \times 10^4$. A Krylov-Schur iteration procedure from the SLEPC package [31] has been used. Since we are interested in the low part of the spectrum, in order to reduce the time of calculation only the first n eigenvalues [with $n \sim (1\text{–}2) \times 10^3$] are calculated. In the evaluation of the first moment (6) we need to know all the excited states, and SRPA calculations with high energy cutoff for $2p2h$ configurations would require a very long calculation time. Therefore, we have done some calculations with a smaller energy cutoff, that is, $E_{\mathrm{cut}} = 60$ MeV, so that the whole energy spectrum can be calculated. In Table I we report, for the monopole case, the isoscalar and isovector values (second and third columns, respectively) of the SRPA first moment

$$m_1 = \sum_\nu^{\omega_{\max}} \omega_\nu |\langle \nu | F | 0 \rangle|^2 \tag{14}$$

obtained by including all the states with an excitation energy lower than $\omega_{\max}$, whose increasing values are shown in the first column of the table. In the last row, the corresponding RPA values are reported with $\omega_{\max} = 100$ MeV. We see that, with increase of the value of the parameter $\omega_{\max}$, the SRPA values of the first moment become close to the RPA ones. Similar results have also been obtained in the quadrupole and dipole cases.

We stress that, for even smaller values of the energy cutoff E_{cut}, a similar (almost identical) agreement of the SRPA m_1 with the RPA value is found. Indeed, a change in the energy cutoff E_{cut} causes only a redistribution of the strength while the total strength is the same and is equal to the RPA value. This is related on the one hand to the fact that only the $1p1h$ amplitudes appear in the transition amplitudes and on the other hand to the formal properties of the SRPA equations [27].

A similar behavior is found when SRPA calculations are performed with the rearrangement terms as they are defined in

TABLE II. As in Table I but SRPA results include also the rearrangement terms.

ω_{max}	$m_1(T=0)$ SRPA*	$m_1(T=1)$ SRPA*
40	616.6714	119.7808
50	650.1523	155.1027
60	663.9445	181.1740
70	670.0688	185.2818
80	670.2844	197.3268
90	671.5175	200.6471
100	671.6515	201.2493
110	671.6515	201.2493
RPA	671.6516	201.2494

RPA included. In Table II are shown the results so obtained. In this case we see also that the total SRPA moments, that is, the ones corresponding to the largest value of the parameter ω_{max}, are the same as the ones shown in Table I. At the same time, we stress that a different distribution with respect to the ω_{max} energy is found (see also Fig. 6).

IV. SECOND RANDOM-PHASE APPROXIMATION EXCITATION SPECTRUM IN ^{16}O

In this section, we present the nuclear strength distributions obtained in the SRPA for different multipolarities and compare them with the RPA ones. The doubly magic nucleus ^{16}O has been chosen for these first applications of the Skyrme SRPA. In the SRPA different levels of approximation will be considered. As discussed previously, in the case of density-dependent interactions it is not clear how to define the residual interaction appearing in the matrix elements beyond the RPA, in particular as far as the rearrangement terms are concerned. Work is in progress to derive the proper expressions to be used in matrix elements beyond the RPA; however, we believe that useful information can be obtained by using two different choices: (i) The interaction is used without rearrangement terms in matrix elements beyond the RPA; (ii) rearrangement terms are included also in matrix elements beyond the RPA, calculated with the usual RPA prescription.

Furthermore, the full SRPA calculations are compared with those obtained when the diagonal approximation is used.

A. Monopole and quadrupole strength distributions

In this section, we focus our attention on the monopole and quadrupole strength distributions. Unless otherwise stated, no rearrangement terms are included in SRPA calculations. In Fig. 3 we show the RPA (dashed black lines) and SRPA (full red lines) results for the isoscalar (upper panel) and isovector (lower panel) monopole strength distributions. In the SRPA all the $2p2h$ configurations with an unperturbed energy lower than an energy cutoff $E_{cut} = 120$ MeV are included.

In both isoscalar and isovector cases, the strongest effect in the SRPA is a several-MeV shift of the strength distribution to lower energies with respect to the RPA. This result seems to

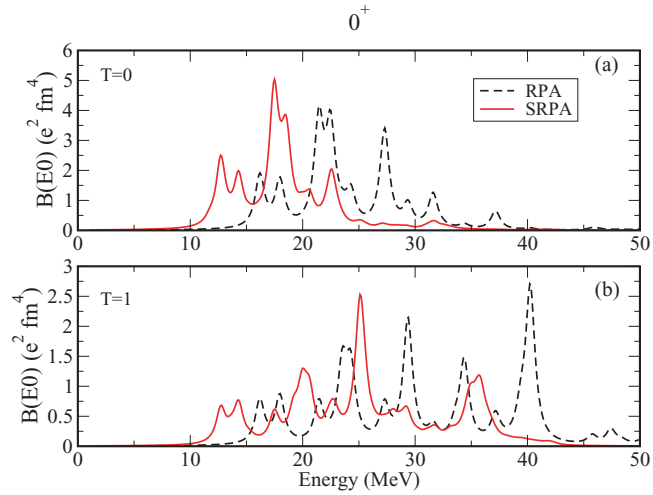

FIG. 3. (Color online) RPA [dashed (black) lines] and SRPA [full (red) lines] for the isoscalar (upper panel) and isovector (lower panel) monopole strength distributions.

be a general feature of the SRPA and has been found also in different SRPA calculations [18–20]. Looking at the figures, however, one sees that the profiles of the strength distributions are not very much changed, except for this shift. The same remarks are valid also for the quadrupole case displayed in Fig. 4. Figure 5 gives an idea of the detail in which the SRPA describes the fine structure of the response: a very dense distribution of discrete contributions can be seen for the SRPA case owing to the existence of many $2p2h$ elementary excitations in addition to the standard RPA $1p1h$ ones.

Figures 6 and 7 represent the same quantities as Figs. 3 and 4, respectively. However, this time the SRPA results obtained with rearrangement terms in beyond-RPA matrix elements (SRPA$^{(*)}$) are also presented in order to evaluate their effect.

For the isoscalar monopole case (top panel of Fig. 6), the residual interaction seems to be more repulsive when rearrangement terms are added, providing a smaller energy shift to lower energies with respect to the RPA. In all the

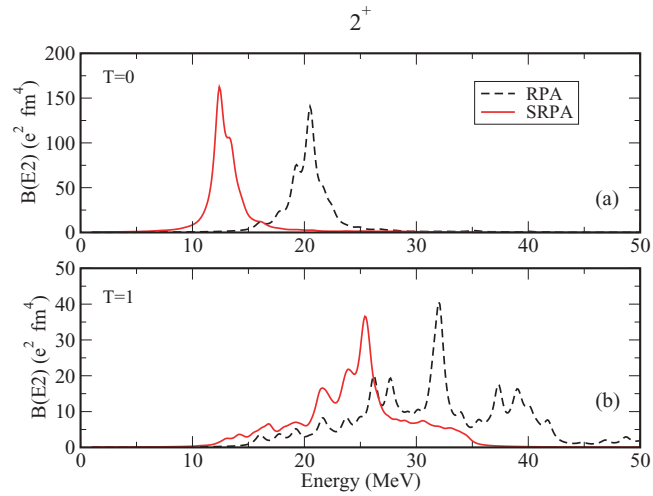

FIG. 4. (Color online) As Fig. 3 but for the quadrupole case.

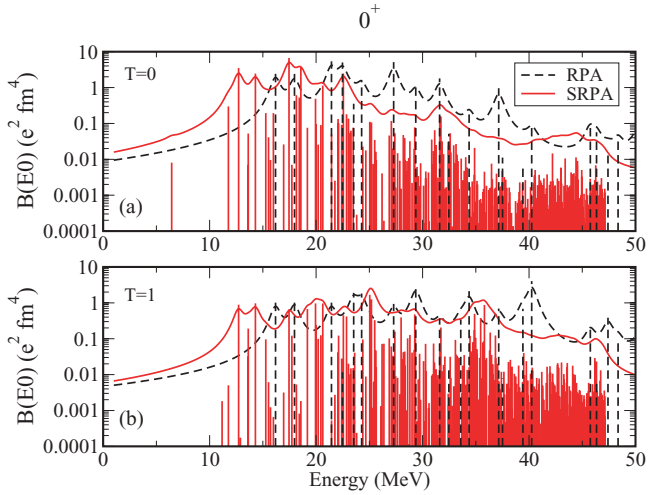

FIG. 5. (Color online) As Fig. 3 but using a logarithmic scale in the ordinate.

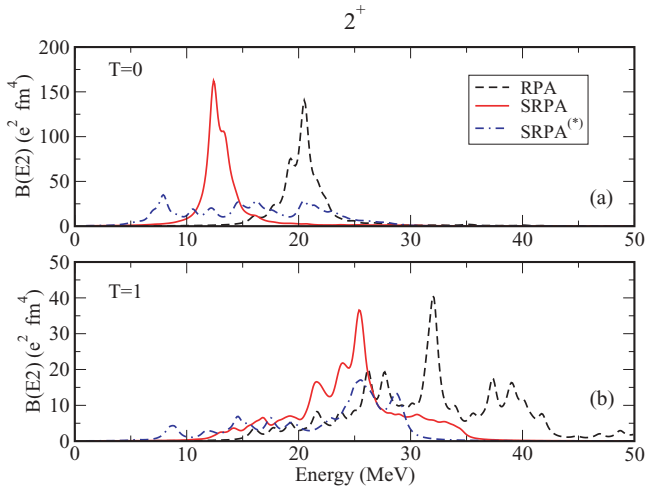

FIG. 7. (Color online) As Fig. 6 but for the quadrupole case.

other cases shown in Figs. 6 and 7, the strength distribution appears very strongly fragmented when rearrangement terms are included in all matrix elements. We know that the usually adopted way to evaluate the rearrangement terms in beyond-RPA matrix elements is not the correct one even if it is currently used. Work is in progress to obtain the correct expressions; the fact that the SRPA$^{(*)}$ results are so different from the SRPA ones underlines that this is a very delicate point and indicates that the proper expressions are needed.

In Figs. 8 and 9 the comparison is made with the diagonal approximation. The results are quite different, and this suggests that the residual interaction should not be neglected in the matrix A_{22} in Skyrme-SRPA calculations.

Finally, Figs. 10–13 display the transition densities. In Fig. 10 (for the monopole isoscalar response) the SRPA transition density refers to the peak at ∼17 MeV while the RPA transition density is evaluated for the peak at ∼21 MeV in the top panel of Fig. 3. The profiles are not very different, meaning that the nature of these RPA and SRPA excited states is not very different in terms of the spatial distributions of wave functions contributing to them. The same considerations can be made for the results shown in Fig. 12 (referring to the quadrupole isoscalar response). In this figure, the RPA (SRPA) transition density is calculated for the peak at ∼22 MeV (13 MeV) in the top panel of Fig. 4.

The case for the isovector responses is different. In Fig. 11 the RPA (SRPA) transition density, for the monopole response, is calculated for the peak at ∼29 MeV (25 MeV) shown in the bottom panel of Fig. 3. For the quadrupole case, the transition densities obtained in the RPA (SRPA) for the peak at ∼32 MeV (25 MeV) (see lower panel of Fig. 4) are shown in Fig. 13. Important differences are visible between RPA

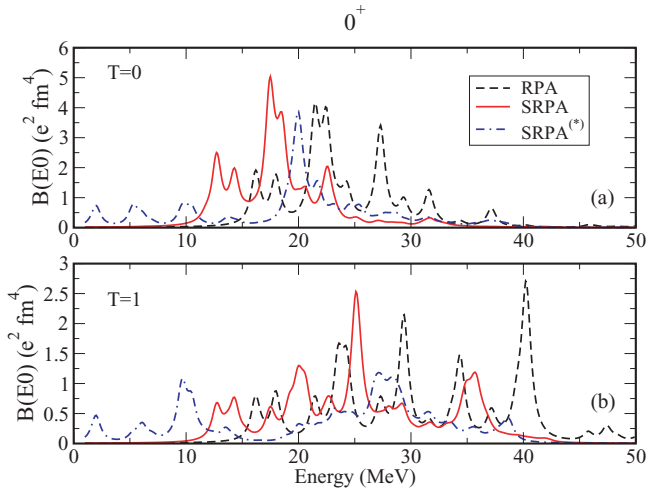

FIG. 6. (Color online) Comparison between RPA [dashed (black) lines], SRPA [full (red) lines], and SRPA with rearrangements terms [dot-dashed (blue) lines]. The isoscalar (upper panel) and isovector (lower panel) monopole strength distributions are shown.

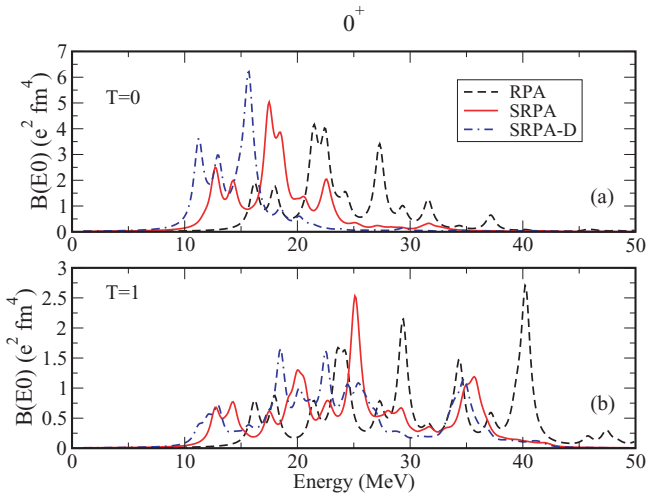

FIG. 8. (Color online) Comparison between RPA [dashed (black) lines], SRPA [full (red) lines], and SRPA in the diagonal approximation [dot-dashed (blue) lines]. The isoscalar (upper panel) and isovector (lower panel) monopole strength distributions are shown.

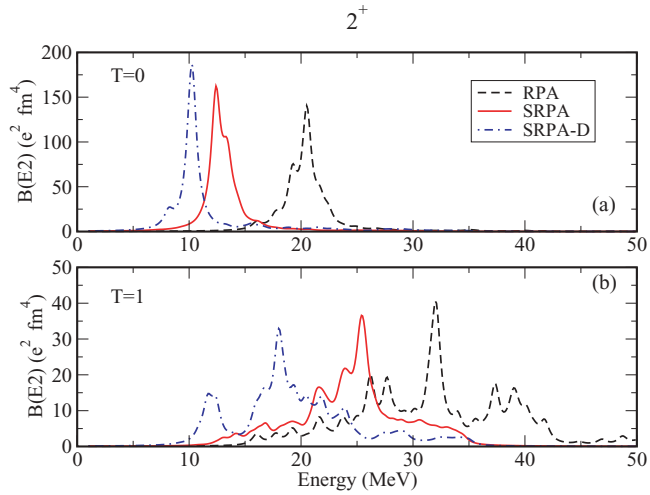

FIG. 9. (Color online) As Fig. 8 but for the quadrupole case.

and SRPA results, suggesting that the nature of SRPA and RPA excited states in terms of the radial distribution of wave functions contributing to the excitation is quite different.

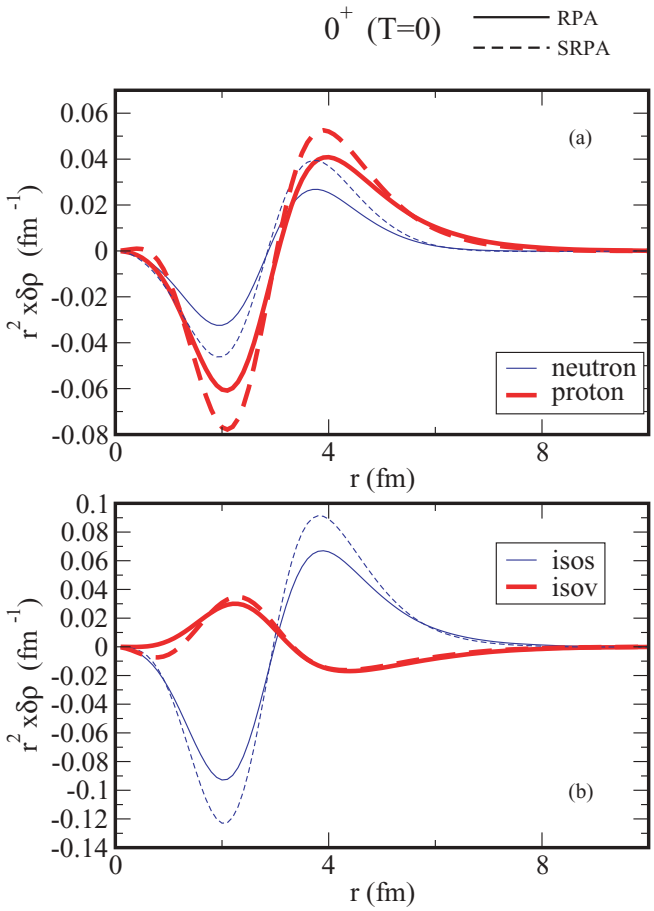

FIG. 10. (Color online) Comparison between RPA (full lines) and SRPA (dotted lines) transition densities for the monopole isoscalar states (see text): (a) for neutrons (thin lines) and protons (bold lines); (b) for isoscalar (thin lines) and isovector (bold lines) cases. See text for more details.

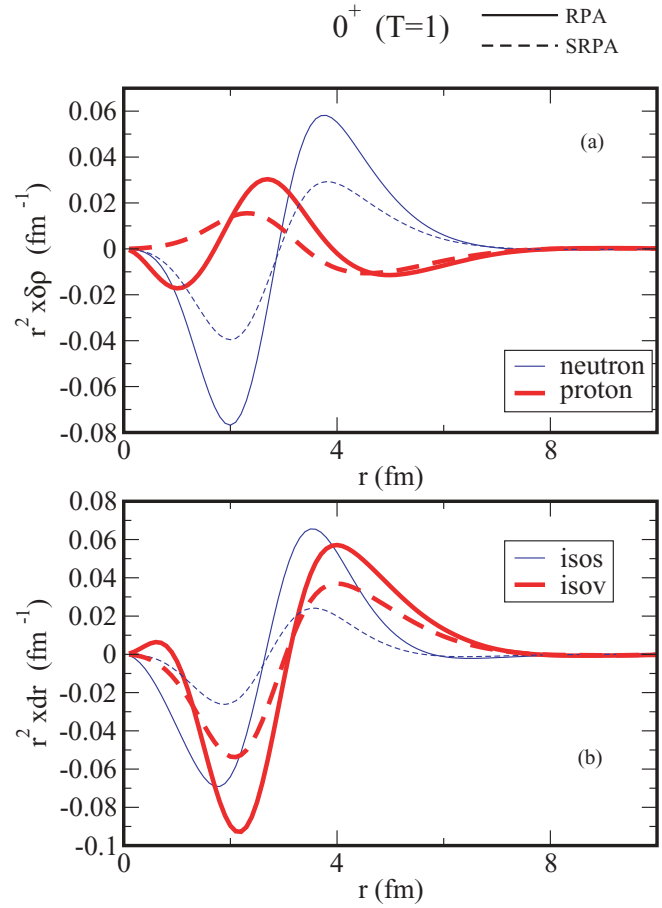

FIG. 11. (Color online) As Fig. 10 but for the monopole isovector states.

B. Dipole strength distributions

The Thouless theorem on the EWSRs [32] is a very important feature of the RPA and it holds also in the SRPA [3]. It guarantees that spurious excitations corresponding to broken symmetries separate out and are orthogonal to the physical states. In Ref. [33] a detailed discussion about the treatment of single and double spurious modes in the RPA and extended RPA theories has been presented. In particular, it has been shown that, when an approximate ground state is used and/or $2p2h$ configurations are included, all the single-particle amplitudes have to be taken into account for the construction of the elementary configurations in order to have single and double spurious modes lying at zero energy. In a self-consistent RPA, that is, when the same interaction is used at HF and RPA level, the motion of the center of mass (associated with the translational invariance) appears at zero energy and is thus exactly separated from the physical spectrum. As we have mentioned, our RPA approach is not fully self-consistent and the spurious state lies at about 1 MeV, exhausting more than 96% of the isoscalar EWSRs. In the SRPA, as a consequence of the coupling with the $2p2h$ configurations, the spurious state is found to be at imaginary energy. We stress that in a self-consistent SRPA approach this state should appear at zero energy as in the RPA. In order to study the possible mixing with spurious components, we have examined the isoscalar

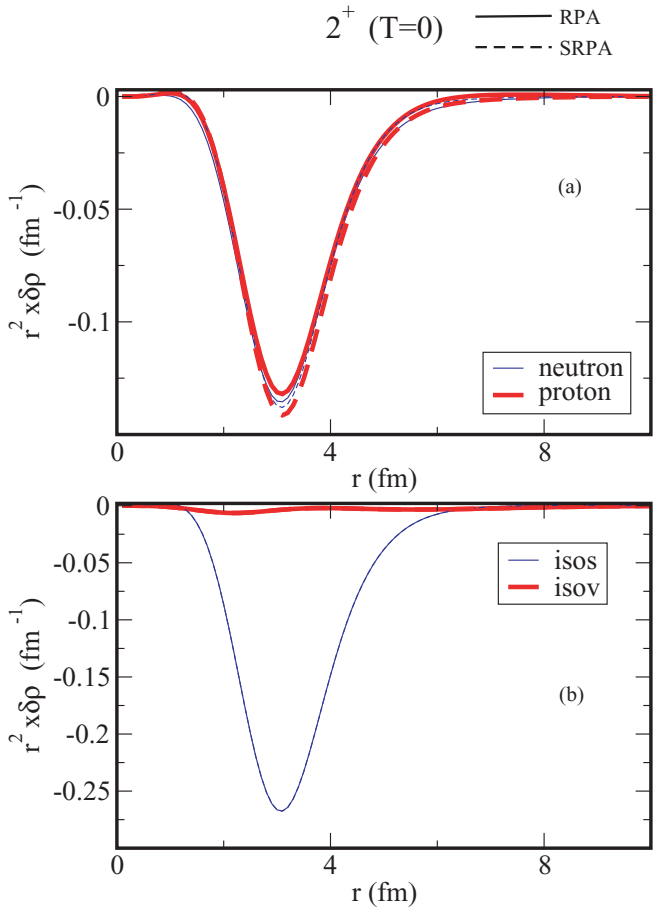

FIG. 12. (Color online) Comparison between RPA (full lines) and SRPA (dotted lines) transition densities for the quadrupole isoscalar states (see text): (a) neutrons (thin lines) and protons (bold lines); (b) isoscalar (thin lines) and isovector (bold lines) cases. See text for more details.

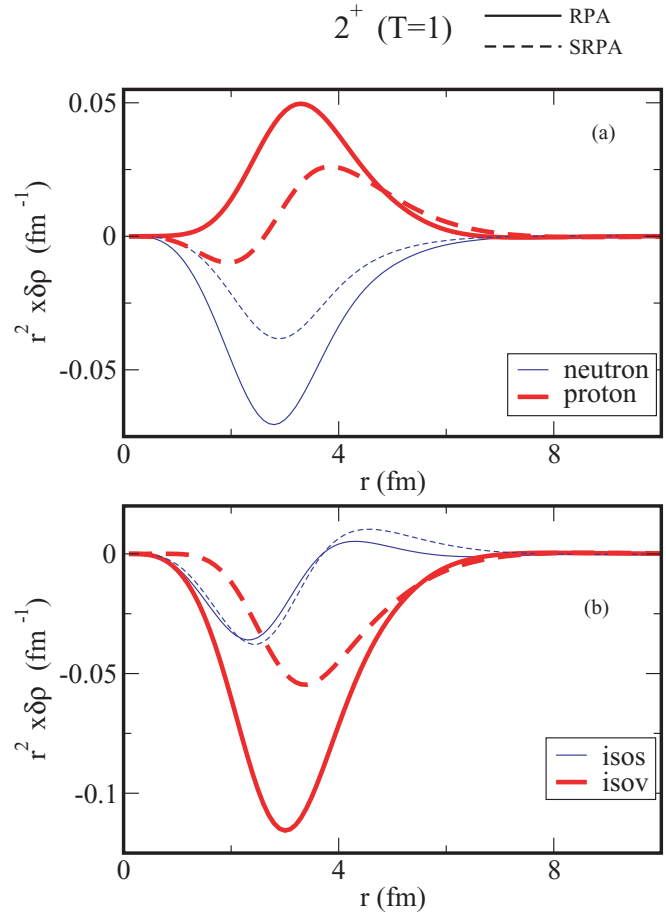

FIG. 13. (Color online) As Fig. 12 but for the quadrupole isovector case.

dipole strength distribution using a transition operator of the radial form ($\sim r^3$) and its corrected form ($\sim r^3 - \frac{5}{3}\langle r^2\rangle r$). The results are shown in the upper panel of Fig. 14. We can see that some differences between the two cases appear, especially in the lowest part of the spectrum, while the mixing with spurious components is smaller in the energy region around and beyond the isovector dipole giant resonance. Recall that a prescription often used in the literature for the treatment of the spurious mode consists in multiplying the residual interaction by a renormalizing factor such that the spurious mode is found at zero energy. In our RPA calculations, the spurious state is found at 1.02 MeV, and by use of a renormalizing factor of 1.006 its energy goes down to 0.02 MeV; the rest of the isoscalar and isovector distributions remain practically unchanged. The same prescription has not been used in the SRPA since the use of a renormalizing factor does not solve the problem of the appearance of imaginary solutions, even when larger values of the renormalizing factor are used.

In the lower panel of Fig. 14 we plot the results for the isovector case. We observe that, in going from the RPA to the SRPA, as in the monopole and quadrupole cases, there is a strong shift toward lower energies of the strength distribution.

In Fig. 15, we show the results when the diagonal approximation is used. In the upper panel of the figure, the isoscalar strength distributions obtained using the corrected and uncorrected transition operators are shown, and we see that, as in the previous case, very small differences are present when the two different operators are used. In the lower panel of the same figure, the isovector distributions obtained in the RPA (dashed black line), the SRPA in the diagonal approximation (dot-dashed blue line), and the full SRPA (full red line) are shown. It is interesting to note that the results obtained in the diagonal approximation are different from the ones obtained in the full SRPA, the differences, however, being smaller than the ones found in the monopole and quadrupole cases.

As far as the rearrangement terms are concerned, we have found in the dipole case that, even when small values of the $2p2h$ energy cutoff $E_{\rm cut}$ are used (60–80 MeV), the SRPA equations give imaginary solutions if the rearrangement terms are included in all matrix elements. Moreover, a comparison in this case of the isoscalar strength distributions obtained by using the corrected and uncorrected transition operators shows very large differences, especially in the low-energy part of the spectrum, indicating that a strong mixing with spurious components is present in this case. In the isovector channel, the position of the main peak is not very different from the one obtained when no rearrangement terms are used (lower

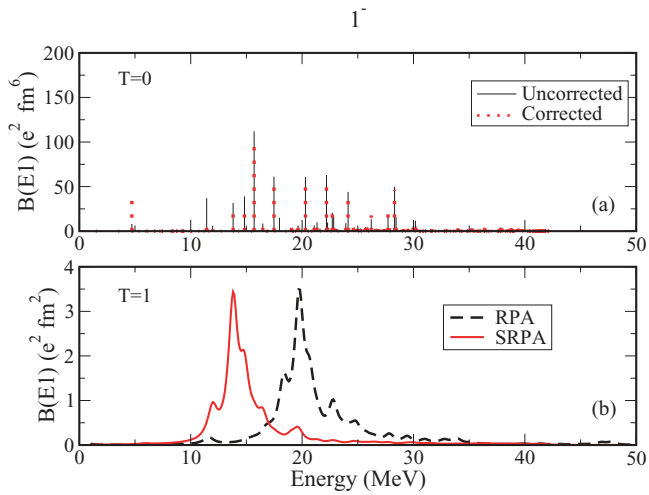

FIG. 14. (Color online) Upper panel: SRPA isoscalar dipole strength distribution obtained with a transition operator of radial form ($\sim r^3$) [full (black) lines], and its form $\sim r^3 - (5/3)\langle r^2\rangle r$ [dotted (red) lines] corrected to take into account c.m. corrections. Lower panel: RPA [dashed (black) line] and SRPA [full (red) line] isovector dipole strength distribution obtained using the standard dipole transition operator of radial form ($\sim r$).

panel of Fig. 14), but the height of the peak is strongly reduced (more than 50%).

In Fig. 16 the RPA (SRPA) transition density, for the isovector dipole response, is calculated for the peak at ∼20 MeV (14 MeV) shown in the bottom panel of Fig. 14. We see that in the dipole case the transition densities in the RPA and SRPA are quite similar. This behavior is at variance

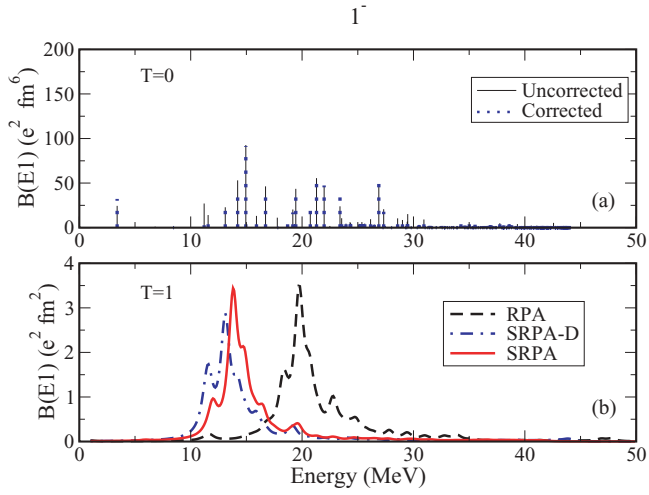

FIG. 15. (Color online) Upper panel: Isoscalar dipole strength distribution obtained within the SRPA in the diagonal approximation using a transition operator of radial form ($\sim r^3$) [full (black) lines] and its form [dotted (blue) lines] form $\sim r^3 - (5/3)\langle r^2\rangle r$ corrected to take into account c.m. corrections. Lower panel: RPA [dashed (black) line], SRPA in the diagonal approximation [dot-dashed (blue) line], and full SRPA [full (red) line] isovector dipole strength distribution obtained using the standard dipole transition operator of radial form ($\sim r$).

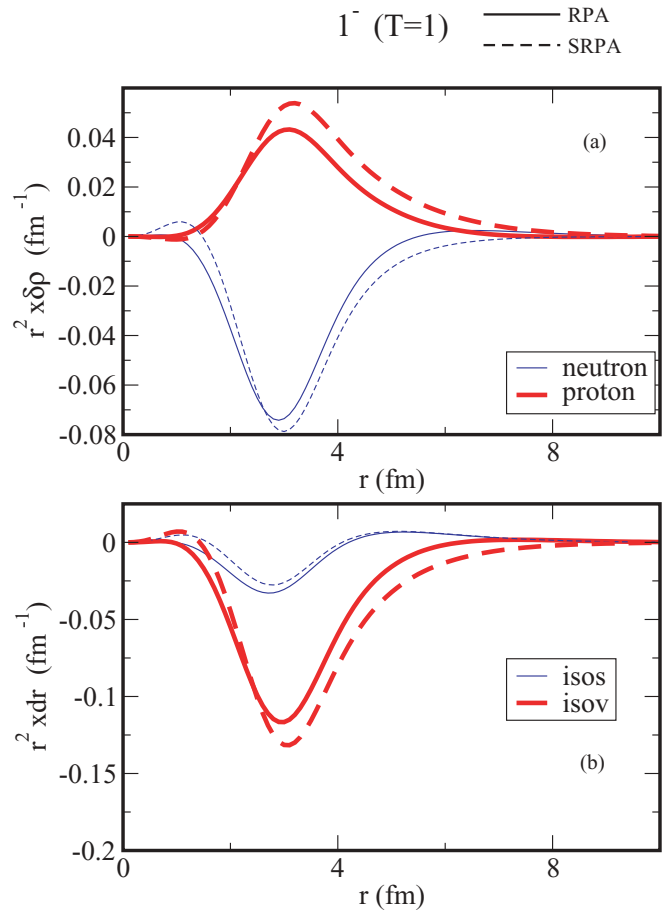

FIG. 16. (Color online) As Fig. 12 but for the dipole isovector case.

with what we found in the monopole and quadrupole cases, as shown in Figs. 11 and 13, respectively.

C. Low-lying 0^+ and 2^+ states

The results for the 0^+ and 2^+ low-lying states obtained in the SRPA are shown in Tables III and IV. These states are mainly composed by $2p2h$ configurations.

The largest $1p1h$ configuration in the 0^+ state is $(2p_{1/2}, 1p_{1/2})^{\pi}$ with an unperturbed energy of 16.17 MeV when no rearrangement terms are considered and $(3p_{1/2}, 1p_{1/2})^{\nu}$ with an unperturbed energy of 24.03 MeV when rearrangement

TABLE III. Energy of the lowest 0^+ state obtained in the RPA and SRPA, compared with the experimental value [34]. The results identified with the star are obtained by taking into account rearrangement terms (last two rows). By "SRPA-D" we indicate the SRPA results when the diagonal approximation is used (fourth and sixth rows). The SRPA result in the diagonal approximation with rearrangement terms gives an imaginary solution (last row).

Low-lying 0^+ energy (MeV)					
Expt.	RPA	SRPA	SRPA-D	SRPA*	SRPA*-D
∼6	16.19	6.43	11.23	5.29	Imaginary

TABLE IV. As Table III but for the 2^+ state.

Low-lying 2^+ energy (MeV)					
Expt.	RPA	SRPA	SRPA-D	SRPA*	SRPA*-D
∼7	16.03	7.16	12.44	4.70	Imaginary

terms are included. In both cases, the lowest $2p2h$ configuration is $[(1d_{5/2}, 1p_{1/2})^3[(1d_{5/2}, 1p_{1/2})^3]^0_\pi$ with an unperturbed energy of E =15.26 MeV.

For the 2^+ state, the most important $1p1h$ configuration is $(2d_{5/2}, 1s_{1/2})^\pi$ with an unperturbed energy of 28.28 MeV when rearrangement terms are not considered. When rearrangement terms are included, the most important configuration is $(2p_{3/2}, 1p_{1/2})^\nu$ with an unperturbed energy of 21.71 MeV. The lowest $2p2h$ configuration is, in both cases, $[(1d_{5/2}, 1p_{1/2})^3[(1d_{5/2}, 1p_{1/2})^3]^2_\pi$ with an unperturbed energy of 15.26 MeV.

Several conclusions may be drawn about these results. First, the RPA is not able to describe these low-lying states at all, simply because beyond-$1p1h$ configurations are necessary to construct them. The RPA energies are indeed far too high in both cases.

It is striking that the SRPA energies are very close to the experimental results. The residual interaction seems to be very important for describing these states: The first unperturbed $2p2h$ configuration is actually located at about 15 MeV, and the residual interaction is thus responsible for the strong shift to lower energies in the response. When rearrangement terms are included, the shift is even stronger. The diagonal approximation looks very poor for the treatment of these low-energy states, indicating that the interaction between $2p2h$ configurations is very important for providing the correct excitation energies.

Finally, it is interesting to compare the SRPA results with those from other types of analysis. As an illustration, let us consider the energy of the first 0^+ excited state. *Ab initio* coupled-cluster investigations do not reproduce at all the energy of this state, providing an excitation energy of 19.8 MeV [35]. Brown and Green have described the low-lying states in ^{16}O by mixing spherical and deformed states [36]. The shell model can nicely describe these states owing to the configuration mixing [37]. Cluster models are also able to well describe this state by assuming an $\alpha+^{12}$C or a 4α structure for the nucleus ^{16}O (see Ref. [38] and references therein). The SRPA is the only RPA-like approach in spherical symmetry that reproduces this energy without any special modelization for the structure of the nucleus ^{16}O.

It is worth mentioning, however, that a complete analysis of these low-energy states would need also the evaluation of the $B(E\lambda)$ values. Work is in progress in this direction to evaluate the transition probabilities in these cases, where the excitations are mainly composed of $2p2h$ configurations and thus a transition operator containing also a two-body part should be more suitable, as in Ref. [19] in the case of the double dipole resonance.

V. CONCLUSIONS

We have performed Skyrme-SRPA calculations for describing collective and low-lying excited states in ^{16}O. The Skyrme interaction SGII is used. The SRPA scheme is fully treated without employing the currently used second Tamm-Dancoff or diagonal approximations. The rearrangement terms of the residual interaction are treated in this work (i) by neglecting them in the matrix elements beyond the RPA; (ii) by calculating them with the usual RPA procedure for all the matrix elements. Work is in progress to derive the proper expressions to be used in beyond-RPA matrix elements.

A general feature of the SRPA strength distributions for giant resonances is a several-MeV shift to lower energies with respect to RPA distributions. This shift is very strong, so Skyrme-SRPA energies of giant resonances are typically too low with respect to the experimental response (Skyrme-RPA results are in general in good agreement with the experimental data for these excitations). However, the SRPA energies of the low-lying 0^+ and 2^+ states are in very good agreement with the experimental results. Actually, these excitations are totally missing in the RPA spectrum because they are mainly composed of $2p$-$2h$ configurations. The situation is thus very different from the case of giant resonances, where the excited modes are in any case mainly composed of $1p1h$ configurations and can be described by both models.

To cure the problem of the strong energy shift for giant resonances, we plan to explore the possibility of using an extended SRPA scheme along the lines of Refs. [20,39]. Since the giant resonances and the low-lying states treated here are basically very different (composed of $1p1h$ and $2p2h$ excitations, respectively) and are related to different kinds of matrix elements, one can eventually expect an extended SRPA model to solve the problem of the strong shift of giant resonances, preserving at the same time the good quality of the low-lying states. A longer-term project is to look for some new parametrization of the effective interaction, adjusted so as to make it suitable for SRPA calculations.

Finally, after this first numerical application of the method, we plan in future work to explore with the SRPA heavier or more exotic nuclei and to check the model dependence of the results by employing other Skyrme parametrizations also.

ACKNOWLEDGMENTS

The authors gratefully thank P. Papakonstantinou, N. Pillet, P. Schuck, N. Van Giai, and M. Tohyama for fruitful discussions.

[1] P. Ring and P. Schuck, *The Nuclear Many-Body Problem* (Springer-Verlag, Berlin, 1980); E. Khan, N. Sandulescu, M. Grasso, and N. V. Giai, Phys. Rev. C **66**, 024309 (2002).

[2] D. Gambacurta, F. Catara, and M. Grasso, Phys. Rev. C **80**, 014303 (2009).

[3] C. Yannouleas, Phys. Rev. C **35**, 1159 (1987).

[4] J. da Providencia, Nucl. Phys. **61**, 87 (1965).
[5] M. Tohyama and M. Gong, Z. Phys. A **332**, 269 (1989).
[6] D. Lacroix, S. Ayik, and Ph. Chomaz, Prog. Part. Nucl. Phys. **52**, 497 (2004).
[7] T. Hoshino and A. Arima, Phys. Rev. Lett. **37**, 266 (1976).
[8] W. Knupfer and M. G. Huber, Z. Phys. A **276**, 99 (1976).
[9] S. Nishizaki and J. Wambach, Phys. Lett. B **349**, 7 (1995).
[10] S. Nishizaki and J. Wambach, Phys. Rev. C **57**, 1515 (1998).
[11] S. Adachi and S. Yoshida, Nucl. Phys. A **306**, 53 (1978).
[12] B. Schwesinger and J. Wambach, Phys. Lett. B **134**, 29 (1984).
[13] B. Schwesinger and J. Wambach, Nucl. Phys. A **426**, 253 (1984).
[14] S. Drozdz, V. Klent, J. Speth, and J. Wambach, Nucl. Phys. A **451**, 11 (1986).
[15] S. Drozdz, V. Klent, J. Speth, and J. Wambach, Phys. Lett. B **166**, 18 (1986).
[16] C. Yannouleas, M. Dworzecka, and J. J. Griffin, Nucl. Phys. A **397**, 239 (1983).
[17] C. Yannouleas and S. Jang, Nucl. Phys. A **455**, 40 (1986).
[18] P. Papakonstantinou and R. Roth, Phys. Lett. B **671**, 356 (2009).
[19] P. Papakonstantinou and R. Roth, Phys. Rev. C **81**, 024317 (2010).
[20] D. Gambacurta and F. Catara, Phys. Rev. B **79**, 085403 (2009).
[21] N. Van Giai and H. Sagawa, Phys. Lett. B **106**, 379 (1981); Nucl. Phys. A **371**, 1 (1981).
[22] E. Litvinova, P. Ring, and V. Tselyaev, Phys. Rev. C **78**, 014312 (2008); G. Tertychny, V. Tselyaev, S. Kamerdzhiev, F. Krewald, J. Speth, E. Litvinova, and A. Avdeenkov, Nucl. Phys. A **788**, 159 (2007); G. Colò, H. Sagawa, N. Van Giai, P. F. Bortignon, and T. Suzuki, Phys. Rev. C **57**, 3049 (1998); G. Colò, N. Van Giai, P. F. Bortignon, and R. A. Broglia, *ibid.* **50**, 1496 (1994).
[23] Ph. Chomaz and N. Frascaria, Phys. Rep. **252**, 275 (1995); K. Boretzky *et al.*, Phys. Rev. C **68**, 024317 (2003); M. Fallot *et al.*, Nucl. Phys. A **729**, 699 (2003).
[24] E. G. Lanza, F. Catara, D. Gambacurta, M. V. Andrés, and Ph. Chomaz, Phys. Rev. C **79**, 054615 (2009).
[25] S. Adachi and S. Yoshida, Phys. Lett. B **81**, 98 (1979).
[26] S. Adachi and S. Yoshida, Nucl. Phys. A **462**, 61 (1987).
[27] S. Adachi, E. Lipparini, Nucl. Phys. A **489**, 445 (1988).
[28] G. Lauritsch and P. G. Reinhard, Nucl. Phys. A **509**, 287 (1990); K. Takayanagi, K. Shimizu, and A. Arima, *ibid.* **477**, 205 (1988); A. Mariano, F. Krmpotic, and A. F. R. de Toledo Piza, Phys. Rev. C **49**, 2824 (1994).
[29] D. Gambacurta, M. Grasso, F. Catara, and M. Sambataro, Phys. Rev. C **73**, 024319 (2006).
[30] G. Colò, N. Van Giai, P. F. Bortignon, and R. A. Broglia, Phys. Rev. C **50**, 1496 (1994).
[31] V. Hernandez, J. E. Roman, and V. Vidal, ACM Trans. Math. Softw. **31**, 351 (2005), [http://www.grycap.upv.es/slepc].
[32] D. J. Thouless, Nucl. Phys. **21**, 225 (1960).
[33] M. Tohyama and P. Schuck, Eur. Phys. J. A **19**, 203 (2004).
[34] F. Ajzenberg-Selove, Nucl. Phys. A **375**, 1 (1982); O. Sorlin and M. G. Porquet, Prog. Part. Nucl. Phys. **61**, 602 (2008).
[35] M. Wloch, D. J. Dean, J. R. Gour, M. Hjorth-Jensen, K. Kowalski, T. Papenbrock, and P. Piecuch, Phys. Rev. Lett. **94**, 212501 (2005).
[36] G. E. Brown and A. M. Green, Nucl. Phys. **75**, 401 (1966).
[37] A. P. Zuker, B. Buck, and J. B. McGrory, Phys. Rev. Lett. **21**, 39 (1968).
[38] Y. Funaki, T. Yamada, H. I. Horiuchi, G. Ropke, P. Schuck, and A. Tohsaki, Phys. Rev. Lett. **101**, 082502 (2008).
[39] D. Gambacurta and F. Catara, Phys. Rev. B **81**, 085418 (2010).